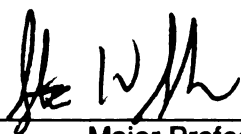This is to certify that the
thesis entitled

Transient Behavior of Centrifugal Pendulum Vibration
Absorbers with Tautochronic Epicycloidal Paths

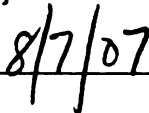presented by

Mark Orlowski

has been accepted towards fulfillment
of the requirements for the

_____M.S._____ degree in _____Mechanical engineering_____

_____
Major Professor's Signature

_____8/7/07_____
Date

MSU is an affirmative-action, equal-opportunity employer

PLACE IN RETURN BOX to remove this checkout from your record.
TO AVOID FINES return on or before date due.
MAY BE RECALLED with earlier due date if requested.

DATE DUE	DATE DUE	DATE DUE

Transient Behavior of Centrifugal Pendulum Vibration Absorbers with Tautochronic Epicycloidal Paths

By
Mark Orlowski

A Thesis

Submitted to
Michigan State University
in partial fulfillment of the requirements
for the degree of

Master of Science

Department of Mechanical Engineering
2007

Abstract

Transient Behavior of Centrifugal Pendulum Vibration Absorbers with Tautochronic Epicycloidal Paths

By
Mark Orlowski

The purpose of this study is to develop a better understanding of transient oscillations in centrifugal pendulum vibration absorbers (CPVAs). A CPVA is a passive device that is used to reduce engine-order torsional vibrations in rotors; it generally consists of a mass that moves along a prescribed path relative to the rotor. The application currently being explored is to decrease torsional vibrations of crankshafts in multi-displacement automobile engines, and determine how CPVAs behave as loading conditions change. The system is modeled as an ideal rotor to which a set of tautochronic, that is, isochronous, CPVAs are attached. Relatively simple and accurate approximate expressions for the maximum transient amplitude of the absorber and the rotor vibration are obtained by considering the linearized system response, and by the method of averaging applied to a weakly nonlinear model. The results are confirmed by simulations of the full system model. The effects of absorber damping, absorber inertia, and absorber tuning on peak transient responses are investigated. It is shown that trade-offs must be considered when selecting these system parameters for optimal transient performance.

To My Mom and Dad

Acknowledgements

Table of Contents

List of Tables

List of Figures

Chapter 1

Introduction

The automotive industry is very interested in developing and optimizing a device that minimizes the torsional oscillations of the crankshaft in their engines, especially those that operate with differing numbers of cylinders under various load and speed conditions. If these torsional vibrations can be minimized, then the vehicles will be allowed to remain in reduced-cylinder mode, known as MDS at DaimlerChrysler, for a wider range of operating conditions. This would improve the fuel economy of these automobiles, since fewer cylinders would be firing over more of their operating range. This wider envelope also has benefits for reducing emissions.

One device well-suited to this purpose is a centrifugal pendulum vibration absorber, which is often abbreviated as CPVA. A CPVA is a mechanism composed of a mass that swings like a pendulum along a prescribed path when it is attached to a spinning rotor. This swinging motion creates a fluctuating counter-torque that can virtually eliminate the torsional vibrations of the rotor, which are from oscillating torque loads. CPVA's have the added benefits of being relatively cheap to manufacture and/or offer better performance when compared to some of the other competing solutions, such as active engine mounts, dampeners, or flywheels. However, a major area of concern is the

1

possible undesirable transient behavior that may be exhibited by these absorbers as they approach steady state operating conditions.

1.1 Motivation

The motivation of this study is to better understand and predict the transient behavior for systems of centrifugal pendulum vibration absorbers. The first step toward this end is to develop the equations of motion for an idealized model of the system of absorbers and the rotor to which they are attached. Simplification of these equations can then be achieved through the use of linearization, which is valid for small vibration amplitudes, and averaging, which offers an improved approximate solution for the weakly nonlinear model. A comparison will be made of the effectiveness of these mathematical tools by contrasting their results with that of a simulation of the full nonlinear equations of motion. The final motivation is to establish some conclusions that describe ways to adjust the parameters of these devices in order to influence the transient behavior toward a more desirable result.

1.2 Background on Centrifugal Pendulum Vibration Absorbers

The first recorded patent of a centrifugal pendulum vibration absorber was in the 1929 in Britain [2]. Their most common uses currently have been in helicopter rotors, light aircraft engines, diesel engine camshafts, and in radial

aircraft engines in World War Two [3]. The most significant distinction between these absorbers and the more familiar frequency tuned absorbers is that centrifugal pendulum vibration absorbers are tuned to a given *order* of rotation, and thus function continuously over virtually all rotor speeds. Another important feature of these vibration absorbers is that they are passive devices whose motion is completely driven by the dynamics of the rotor.

The path of the center of mass of the absorber dictates the linear tuning order of the path of the absorber, as well as the nonlinear behavior of the absorbers. This path can have many variations, but three predominant forms exist: circular, cycloidal, and tautochronic epicycloidal [1]. Simple circular paths have a deficiency in that they exhibit a strong softening nonlinearity, that is, the absorber frequency becomes smaller as its amplitude is increased [14]. A cycloidal path has the absorbers travel along the curve defined by the locus of a point on the rim of a circle as it rolls along a straight line [4]. A cycloidal path has an inherent slight hardening nonlinearity. The tautochronic epicycloidal path is the one considered in this study; it is formed by the curve defined by the locus of a point on the rim of a circle rolling along a second circle [5]. A tautochronic epicycloidal path is neither hardening nor softening, by definition, since the frequency of motion is independent of amplitude, up to the cusp encountered as the trace point touches the base circle [14]. It is this property of remaining linear as the amplitude increases that makes a tautochronic epicycloidal path so desirable for CPVA paths.

1.3 Outline of the Thesis

In the next chapter, a mathematical model is developed to describe the dynamics of the rotor and absorbers. The equations are first scaled to become non-dimensional, and then linearization is used to reduce their complexity and yield a form amenable to linear vibration analysis. The resulting linear equations are solved for the absorber dynamics, in terms of the arc length traveled by the absorber center of mass, and for the rotor dynamics.

The third chapter lays out how the solution to the linear equations of the system can be manipulated using trigonometric identities, so that the maximum transient amplitude of the absorber movement and of the rotor velocity may be obtained relatively easily. In addition, the manner in which the solution of the linear absorber equation decays to steady-state is considered. Finally, the influences of certain system parameters on the transient behavior of the CPVA are considered, in order to assist with design of absorbers.

In the fourth chapter, the method of averaging is used to obtain approximate solutions of the full nonlinear equations of motion. The averaged equations are solved numerically using a Matlab simulation. The results of these simulations are compared with the results of the linear theory and against simulations of the full nonlinear equations. Finally, the trends observed in the previous chapter are reconsidered for this nonlinear model.

The final chapter establishes conclusions gathered through the use of the methodologies established in the previous chapters. It is found that the linear

theory offers a reasonably good approximation for transient dynamic amplitudes, and that the corrections offered by the averaging applied to the weakly nonlinear model are not sufficient to warrant the more complicated analysis. In addition, the final chapter provides a discussion of possible future areas of study which relate to centrifugal pendulum vibration absorbers but are beyond the scope of this thesis.

Chapter 2

Mathematical Model

To properly analyze the dynamics of the rotor and vibration absorber system, a mathematical model must be developed based upon the physical parameters of the system. From this model, possible solutions of the motion of the absorber(s) and rotor may be derived and plotted, as needed for design.

2.1 Assumptions

A few assumptions are made when creating a mathematical model for the absorbers and rotor system. First, the rotor is considered rigid, therefore it cannot bend or deform as a result of the torques applied on it. The rotor is also assumed to rotate about a fixed axis. Also, it is assumed that the absorbers do not make contact with the stops that limit their motion. In addition, all damping sources in the rotor and the absorbers are assumed to be viscous in nature. Finally, the absorbers are taken to be identical and are modeled as point masses moving along specified paths relative to the rotor. This latter assumption is valid for the commonly-used bifilar suspension of these absorbers [1].

6

2.2 Equations of Motion

The idealized model for a system of absorbers moving along prescribed arcs relative to the rotor is depicted in figure 2-1. The equations of motion are presented and described below.

$\theta, \dot{\theta}$

Absorbers

Path

Rotor, J

$T = T_0 + T_\theta \text{Sin}[n\theta]$
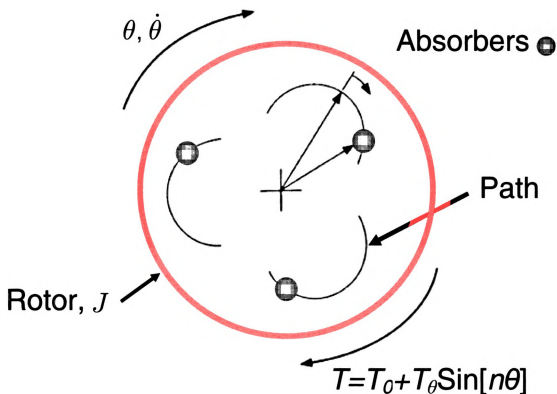
Figure 2-1: Idealized model for a rotor fitted with a system of absorbers.

For a system with N absorbers attached to the rotor, the general equation of motion for the ith absorber is given by [6],

$$m_i \left[\ddot{S}_i + \tilde{G}_i \ddot{\theta} - \frac{1}{2} \frac{dX_i}{dS_i} \dot{\theta}^2 \right] = -c_{ai} \dot{S}_i, \quad i = 1, ..., N \tag{2.1}$$

while the equation of motion for the rotor is,

$$J\ddot{\theta} + \sum_{i=1}^{N} m_i \left[\frac{dX_i}{dS_i} \dot{S}_i \dot{\theta} + X_i \ddot{\theta} + \tilde{G}_i \ddot{S}_i + \frac{d\tilde{G}_i}{dS_i} \dot{S}_i^2 \right] =$$
$$\sum_{i=1}^{N} c_{ai} \tilde{G}_i \dot{S}_i - c_0 \dot{\theta} + T_0 + T_\theta Sin[n\theta], \quad i = 1, ..., N \tag{2.2}$$

The two dynamic variables in the equations of motion for this system are S_i, the arc length position variable for the ith absorber, and θ, the angular orientation of rotor. The system parameters are defined as follows: m_i is the mass of the ith absorber, c_{ai} is the damping value of the ith absorber, J represents the moment of inertia of the rotor, c_0 is the damping value of the rotor, T_0 represents the mean torque acting on the rotor, T_θ is the amplitude of the fluctuating torque, and n is the engine order excitation (which is half the number of cylinders for a four-stroke engine). The function X_i is the square of the function R_i, which is the distance from the rotor center to the position at S_i on the absorber path; this function characterizes the absorber path, as shown in Figure 2.1. The function $\tilde{G}_i$ also relates to the path; it and X_i are described in more detail below. For one tautochronic epicycloidal path absorber, X is given by,

8

$$X(S) = \left(\frac{\rho_0}{1 - \frac{\tilde{n}^2}{\tilde{n}^2 + 1}} \left(Sin[\psi] Cos\left[\frac{\tilde{n}}{\sqrt{\tilde{n}^2 + 1}} \psi \right] \right) \right)^2 +$$

$$\left(-R_0 - \frac{\rho_0}{1 - \frac{\tilde{n}^2}{\tilde{n}^2 + 1}} \left(Cos[\psi] Cos\left[\frac{\tilde{n}}{\sqrt{\tilde{n}^2 + 1}} \psi \right] + \frac{\frac{\tilde{n}^2}{\tilde{n}^2 + 1} S}{\rho_0} Sin[\psi] - 1 \right) \right)^2 \qquad (2.3)$$

$$\psi = \frac{\sqrt{\tilde{n}^2 + 1}}{\tilde{n}} ArcSin\left[\frac{\frac{\tilde{n}}{\sqrt{\tilde{n}^2 + 1}} S}{\rho_0} \right]$$

where ñ, referred to as the linear tuning order of the path [6], is

$$\tilde{n} = \sqrt{\frac{R_0 - \rho_o}{\rho_0}} \qquad (2.4)$$

In equation 2.3, ρ_0 stands for the radius of curvature at the vertex for the absorber and R_0 represents the distance from the rotation center to the vertex for the absorber. Thus, the effective length of an equivalent simple point mass pendulum absorber is ρ_0. The function $\tilde{G}$ is defined in terms of X as follows,

$$\tilde{G}(S) = \sqrt{X - \frac{1}{4}\left(\frac{dX}{dS} \right)^2} \qquad (2.5)$$

Finally, $\dfrac{dX}{dS}$ and $\dfrac{d\tilde{G}}{dS}$ are simply the derivatives with respect to S of the expressions given in equations 2.3 and 2.5, respectively. Another important function of the linear tuning order of the path and the distance from the rotation center to the vertex for the absorber is the absorber arc length at which it hits the cusp where the stops are. This cusp point is at,

$$S_{cusp} = \frac{R_0}{\tilde{n}\sqrt{1+\tilde{n}^2}} \tag{2.6}$$

Note that Equation 2.2 shows that the absorbers are not directly coupled to each other, but only indirectly through the rotor. Also, the rotor is driven by the absorbers through the terms in the summation. It is worth noting that the rotor does not react specifically to any individual absorber, but only to the sum of the effects of all absorbers.

2.3 Transformation to Non-dimensional Form

It is possible through a rescaling process and a change of variables to alter equations 2.1 and 2.2 to put them in a non-dimensional form in which the applied torque becomes a periodic excitation, rather than a nonlinearity. First, the independent variables, S_i and $\dot{\theta}$, are transformed to s_i and v, which both vary dynamically with the angular orientation of rotor [6], by the scaling,

10

$$s_i = \frac{S_i}{R_0}, \qquad\qquad v = \frac{\dot{\theta}}{\Omega} \qquad\qquad (2.7)$$

The term Ω represents the average rotor angular velocity. The independent variable has now changed from time to the angular orientation of rotor. Also, the parameter values are adjusted to their non-dimensional forms,

$$\varepsilon_i = \frac{m_i R_{0i}{}^2}{J}, \qquad\qquad \mu_{ai} = \frac{c_{ai}}{m_i \Omega}, \qquad\qquad \mu_0 = \frac{c_0}{J\Omega},$$

$$\Gamma_0 = \frac{T_0}{J\Omega^2}, \qquad\qquad \Gamma_\theta = \frac{T_\theta}{J\Omega^2} \qquad\qquad (2.8)$$

With these new variables and parameters, the equations of motion for the absorbers and rotor become,

$$v s_i'' + [s_i' + \tilde{g}_i]v' - \frac{1}{2}\frac{dx_i}{ds_i}v = -\mu_{ai}s_i', \quad i = 1,...,N \qquad\qquad (2.9)$$

$$\sum_{i=1}^{N} \varepsilon_i \left[\frac{dx_i}{ds_i}s_i'v^2 + x_i vv' + \tilde{g}_i s_i' vv' + \tilde{g}_i s_i'' v^2 + \frac{d\tilde{g}_i}{ds_i}s_i'^2 v^2 \right] + vv'$$

$$= \sum_{i=1}^{N} \varepsilon_i \mu_{ai}\tilde{g}_i s_i'v - \mu_0 v + \Gamma_0 + \Gamma_\theta Sin[n\theta], \quad i = 1,...,N \qquad\qquad (2.10)$$

11

Similar to X, $\dfrac{dX}{dS}$, $\tilde{G}$, and $\dfrac{d\tilde{G}}{dS}$, x, $\dfrac{dx}{ds}$, $\tilde{g}$, and $\dfrac{d\tilde{g}}{ds}$ are all functions of s. The

values of x, $\dfrac{dx}{ds}$, $\tilde{g}$, and $\dfrac{d\tilde{g}}{ds}$ for a tautochronic epicycloidal path simplify to,

$$x(s) = 1 - (\tilde{n}s)^2$$
$$\frac{dx}{ds}(s) = -2\tilde{n}^2 s$$
$$\tilde{g}(s) = \sqrt{1 - (\tilde{n}s)^2 - \frac{1}{4}\left(-2\tilde{n}^2 s\right)^2}$$
$$\frac{d\tilde{g}}{ds}(s) = \frac{-\tilde{n}^2 s - \tilde{n}^4 s}{\sqrt{1 - \tilde{n}^2 s^2 - \tilde{n}^4 s^2}}$$

(2.11)

2.4 Linearized Equations

Linearization can be utilized to simplify the non-dimensional equations of motion. The equations of motion are linearized by assuming $s = \varepsilon \cdot p$, $v = 1 + \varepsilon \cdot w$, and $v' = \varepsilon \cdot w'$, where ε is considered small. The resulting equations are as follows,

$$p_i'' + \mu_a p_i' + \tilde{n}^2 p_i = -w'$$

(2.12)

$$w' = \frac{1}{1+\varepsilon}\left(l_k \Gamma_\theta Sin[kn\theta] - \frac{\varepsilon}{N}\sum_i \left(p_i'' - \mu_a p_i'\right)\right)$$

Equation 2.12 introduces the parameter k, which has either the value one or two, motivated by the MDS engine application. During MDS operation, k will switch between values of one and two as cylinders activate and deactivate, causing the absorber to switch in and out of resonance operation. Additionally, the parameter l_k is introduced which describes how the fluctuating torque changes due to the effects of entering and existing MDS operation. By substituting for the rotor velocity, w', it is possible to derive an equation that isolates the absorber from the rotor dynamics, as follows for a single absorber (the multi-absorber case goes through similarly),

$$p''+\mu_a\left(1+2v\right)p'+\tilde{n}^2\left(1+v\right)p = -l_k\Gamma_\theta Sin[kn\theta]$$

or

$$p''+2\rho\omega_n p'+\omega_n^2 p = -\Gamma Sin[\omega\theta] \qquad (2.13)$$

In equation 2.13, the natural frequency is $\omega_n=\sqrt{(1+v)\tilde{n}^2}$, the excitation frequency is $\omega=kn$, the damping ratio is $\rho=\dfrac{\mu_a\left(1+2v\right)}{2\sqrt{(1+v)\tilde{n}^2}}$, and Γ is the fluctuating torque.

2.5 Solution for a Single Absorber

Equation 2.12 can be solved analytically or numerically through the use of a Matlab simulation. The analytical solution of the equation 2.12 for the scaled absorber response p with $P_0 = p(0)$ and $V_0 = p'(0)$ is as follows,

$$p = e^{-\theta\rho\omega_n} C[2] Cos\left[\theta\sqrt{1-\rho^2}\,\omega_n\right] + e^{-\theta\rho\omega_n} C[1] Sin\left[\theta\sqrt{1-\rho^2}\,\omega_n\right] +$$
$$\frac{\Gamma\left(2\rho\omega Cos[\theta\omega]\omega_n + Sin[\theta\omega]\left(\omega^2 - \omega_n^2\right)\right)}{\omega^4 + 2\left(2\rho^2 - 1\right)\omega^2\omega_n^2 + \omega_n^4}$$

$$C[1] = \frac{\left(-\Gamma\omega\left(\omega^2 + \left(2\rho^2 - 1\right)\omega_n^2\right) + \left(V_0 + P_0\rho\omega_n\right)\left(\omega^4 + 2\left(2\rho^2 - 1\right)\omega^2\omega_n^2 + \omega_n^4\right)\right)}{\left(\sqrt{1-\rho^2}\,\omega_n\left(\omega^4 + 2\left(2\rho^2 - 1\right)\omega^2\omega_n^2 + \omega_n^4\right)\right)}$$

$$C[2] = \frac{-2\Gamma_\theta\rho\omega\omega_n + P_0\left(\omega^4 + 2\left(2\rho^2 - 1\right)\omega^2\omega_n^2 + \omega_n^4\right)}{\omega^4 + 2\left(2\rho^2 - 1\right)\omega^2\omega_n^2 + \omega_n^4} \qquad (2.14)$$

Figure 2-2 shows an example of the plot of the linearized absorber motion versus the angular orientation of the rotor using the solution stated in equation 2.13 with the parameter values set to be those presented in table 2-1. Note that the envelope varies relatively slowly, due to the small damping and nearly resonant forcing.

14

ρ	0.01
Γ	0.05
k	1
n	1.5
ñ	1.51
ε	0.05
P_0	0
V_0	0

Table 2-1: List of system parameter values for figure 2-2
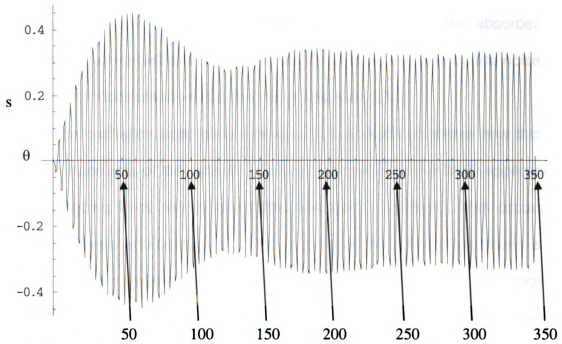
Figure 2-2: Absorber arc length versus rotor angle, simulated using the linearized model.

Equation 2.14 can be broken up into two portions, a transient and a steady state term, as follows:

Transient part:

$$e^{-\theta\rho\omega_n} C[2] Cos\left[\theta\sqrt{1-\rho^2}\,\omega_n\right] + e^{-\theta\rho\omega_n} C[1] Sin\left[\theta\sqrt{1-\rho^2}\,\omega_n\right]$$

Steady State part:

$$\frac{\Gamma\left(2\rho\omega Cos[\theta\omega]\omega_n + Sin[\theta\omega]\left(\omega^2 - \omega_n^2\right)\right)}{\omega^4 + 2\left(2\rho^2 - 1\right)\omega^2\omega_n^2 + \omega_n^4}$$

As long as there is damping present, the transient will decay over time while the steady state portion is constant. The transient is still very important, however, because if the maximum transient value is too large, then the absorber will impact stops, which will affect the absorber's effectiveness and create noise. In fact, it might induce steady-state impacting responses [11].

If the excitation undergoes changes, it is possible to derive how this will affect the transients of the system. An important example for MDS applications is that of going from one steady-state condition to another. This occurs as cylinders activate and deactivate. The most important of these transitions is the one in which the absorbers are initially essentially inactive, and then begin to work when cylinders are taken off-line. For the more general case, the following steps are taken to determine the transient response: First, consider the steady-state response of p for the initial set of forcing parameters. This steady state will provide the set of initial conditions for the ensuing transient response. A nice way to view this is with p and p' in a phase plane plot, such as shown in Figure 2-3.

p'

0.03

0.02

0.01

p

-0.01   -0.005   0.005   0.01

-0.01

-0.02

-0.03
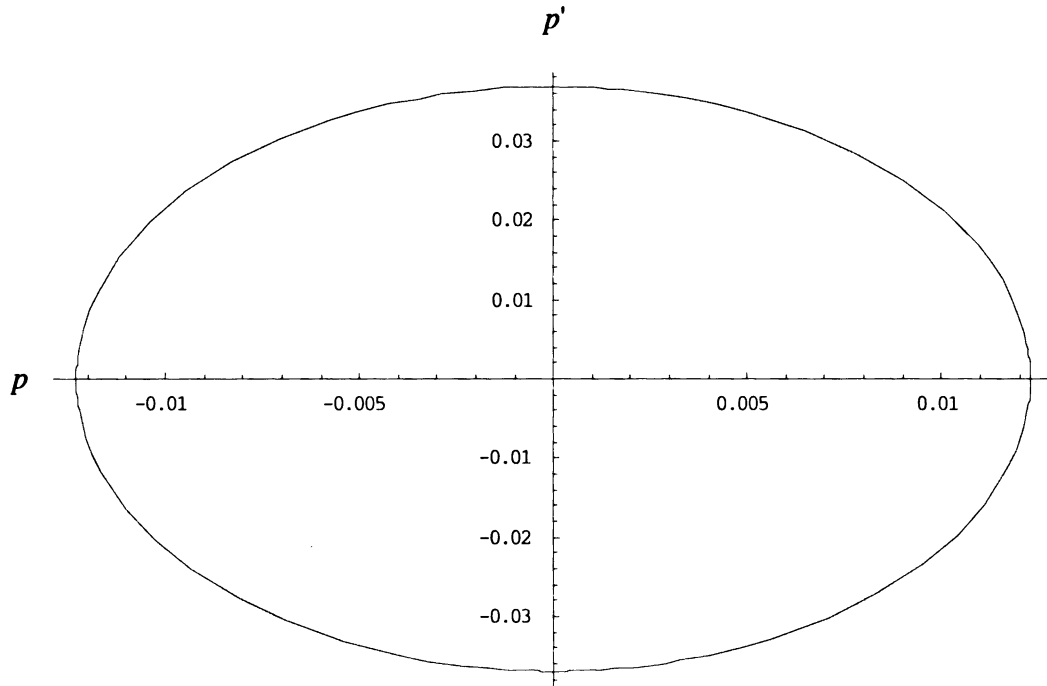
Figure 2-3: Phase plane of the steady-state absorber response from the linearized model; arc-length velocity versus arc-length.

At some instant in time the forcing conditions change, and the initial condition for equation 2.13 is simply the corresponding point on the steady-state ellipse. Different points on the curve will yield different transient solutions since each set of conditions on the curve represents a different phase of the applied torque at which when the change in excitation occurs. The resulting transient takes the response from a starting point on this ellipse and is asymptotic to the steady-state ellipse for the new forcing conditions. Of particular interest is the peak amplitude seen by the absorber and the peak rotor torsional vibration during this transient. This is considered below. Also, note that in MDS engine applications, the starting ellipse is very small, since the excitation amplitude is small and the excitation order is about twice the resonance order. Therefore, a useful and

17

sufficiently accurate approximation can be obtained by assuming zero initial conditions.

2.6 Solution to the Rotor Equation

Once the analytical solution to the linearized absorber equation is developed, its first and second derivatives with respect to θ can be substituted into equation 2.12 to obtain an expression for the linearized rotor response. These derivatives are,

$$p' = C[1]e^{-\theta\rho\omega_n}\sqrt{1-\rho^2}\,\omega_n Cos\left[\theta\sqrt{1-\rho^2}\,\omega_n\right] - C[2]e^{-\theta\rho\omega_n}\rho\omega_n Cos\left[\theta\sqrt{1-\rho^2}\,\omega_n\right] -$$

$$C[1]e^{-\theta\rho\omega_n}\rho\omega_n Sin\left[\theta\sqrt{1-\rho^2}\,\omega_n\right] - C[2]e^{-\theta\rho\omega_n}\sqrt{1-\rho^2}\,\omega_n Sin\left[\theta\sqrt{1-\rho^2}\,\omega_n\right] +$$

$$\frac{\Gamma\omega\left(\left(\omega^2-\omega_n^2\right)Cos[\omega\theta]-2\rho\omega\omega_n Sin[\omega\theta]\right)}{\omega^4+2\left(2\rho^2-1\right)\omega^2\omega_n^2+\omega_n^4}$$

$$p'' = -e^{-\theta\rho\omega_n}\omega_n^2\left(2\rho\sqrt{1-\rho^2}\,C[1]+C[2]-2\rho^2 C[2]\right)Cos\left[\theta\sqrt{1-\rho^2}\,\omega_n\right] -$$

$$e^{-\theta\rho\omega_n}\omega_n^2 C[1]Sin\left[\theta\sqrt{1-\rho^2}\,\omega_n\right] + 2e^{-\theta\rho\omega_n}\rho^2\omega_n^2 C[1]Sin\left[\theta\sqrt{1-\rho^2}\,\omega_n\right] +$$

$$2e^{-\theta\rho\omega_n}\rho\sqrt{1-\rho^2}\,\omega_n^2 C[2]Sin\left[\theta\sqrt{1-\rho^2}\,\omega_n\right] +$$

$$\frac{-\Gamma\omega^4 Sin[\theta\omega]-2\Gamma\rho\omega_n\omega^3 Cos[\theta\omega]+\Gamma_\theta\omega_n^2\omega^2 Sin[\theta\omega]}{\omega^4+2\left(2\rho^2-1\right)\omega^2\omega_n^2+\omega_n^4}$$

$$(2.15)$$

With the substitution of these derivatives and some simplification, the linearized rotor response equation becomes,

$$w' = \frac{1}{1+v} \left\{ \begin{array}{l} \dfrac{\Gamma v \omega \left(2\rho \omega^2 \omega_n + \mu_a (\omega - \omega_n)(\omega + \omega_n)\right) Cos[\omega\theta]}{\omega^4 + 2\left(2\rho^2 - 1\right)\omega^2 \omega_n^2 + \omega_n^4} + \\[2em] \dfrac{\Gamma\left((1+v)\omega^4 + \omega_n^4 + \omega^2 \omega_n \left(-2\mu_a v\rho - \left(2 + v - 4\rho^2\right)\omega_n\right)\right) Sin[\omega\theta]}{\omega^4 + 2\left(2\rho^2 - 1\right)\omega^2 \omega_n^2 + \omega_n^4} + \\[2em] e^{-\rho\omega_n\theta} v\omega_n Cos\left[\sqrt{\rho^2 - 1}\,\omega_n\theta\right] * \\[1em] \left(\mu_a\left(\sqrt{\rho^2 - 1}\,C[1] - \rho C[2]\right) + \omega_n\left(2\rho\sqrt{\rho^2 - 1}\,C[1] + C[2] - 2\rho^2 C[2]\right)\right) + \\[1.5em] e^{-\rho\omega_n\theta} v\omega_n Sin\left[\sqrt{\rho^2 - 1}\,\omega_n\theta\right] * \\[1em] \left(C[1]\left(\omega_n - \rho(\mu_a + 2\rho\omega_n)\right) - C[2]\sqrt{\rho^2 - 1}\,(\mu_a + 2\rho\omega_n)\right) \end{array} \right\} \tag{2.16}$$

The rotor velocity, solved for using integration, is,

$$w = \frac{-1}{1+v} \left[\begin{array}{l} \dfrac{\Gamma Cos[\omega\theta]}{\omega} + \\[1.5em] e^{-\rho\omega_n\theta} v\left(\sqrt{1 - \rho^2}\,\omega_n C[1] - \mu_a C[2] - \rho\omega_n C[2]\right) Cos\left[\sqrt{1 - \rho^2}\,\omega_n\theta\right] + \\[1.5em] \dfrac{\Gamma v \omega\left(\omega^2 - \omega_n(2\mu_a\rho + \omega_n)\right) Cos[\omega\theta]}{\omega^4 + 2\left(2\rho^2 - 1\right)\omega^2 \omega_n^2 + \omega_n^4} + \\[2em] \dfrac{\Gamma v\left(-2\rho\omega^2 \omega_n + \mu_a\left(-\omega^2 + \omega_n^2\right)\right) Sin[\omega\theta]}{\omega^4 + 2\left(2\rho^2 - 1\right)\omega^2 \omega_n^2 + \omega_n^4} - \\[2em] e^{-\rho\omega_n\theta} v\left(\sqrt{1 - \rho^2}\,\omega_n C[2] + \mu_a C[1] + \rho\omega_n C[1]\right) Sin\left[\sqrt{1 - \rho^2}\,\omega_n\theta\right] \end{array} \right] \tag{2.17}$$

Figure 2-4 shows a plot of the rotor response versus θ obtained using equation 2.17 with the parameter values set to be those listed in table 2-1. Again, note

that the response has a relatively slowly varying envelope that settles onto the steady-state.
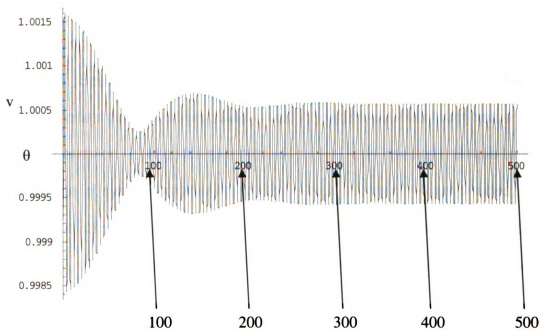
Figure 2-4: Rotor velocity versus crank angle calculated using the linearized model.

Chapter 3

Linear Analysis

Based on the solution developed in the previous chapter, a better understanding of the transient behavior of the absorbers and the rotor can be developed. Specifically, an expression for the envelopes of the absorber and rotor responses can be derived and used to predict the maximum value of the transient behavior. Using this envelope equation, it is relatively simple to study the influence of system parameters on the maximum transient amplitudes. Also, the analysis of the envelope equation yields important information about the decay rate of the transient responses, and how this depends on system parameters.

3.1 Envelope Equation

An envelope equation for the absorber motion can be derived based on the beating phenomenon [7]. By the use of trig identities one can show that,

$$
aSin[\omega_1\theta + \phi_1] + bSin[\omega_2\theta + \phi_2] = \\
\sqrt{a^2 + b^2 + 2abCos[\phi_1 - \phi_2 - (\omega_2 - \omega_1)\theta]}Sin[\omega_1\theta + \Psi]
$$

(3.1)

where the amplitude of the term on the right hand side of the equality in equation 3.1 represents the envelope amplitude, and the phase is not of interest here. Typically, and in the present situation, the two frequencies are relatively close to one another, and the response can be viewed as an oscillation with a slowly varying amplitude and phase. The following additional trigonometric identities are utilized to transform equation 2.14 into a form that matches the left hand side of equation 3.1 [7]:

$$\alpha Sin[\tau\theta] + \beta Cos[\tau\theta] = \sqrt{\alpha^2 + \beta^2} Sin\left[\tau\theta + ArcTan\left[\frac{\beta}{\alpha}\right]\right] \qquad \text{for } \alpha > 0$$

$$\alpha Sin[\tau\theta] + \beta Cos[\tau\theta] = \sqrt{\alpha^2 + \beta^2} Sin\left[\tau\theta + ArcTan\left[\frac{\beta}{\alpha}\right] + \pi\right] \qquad \text{for } \alpha < 0$$

$$\text{(3.2)}$$

This identity must be used twice, once for the transient portion of p and a second time for the steady-state portion. For the transient portion, set $\alpha(\theta)$ equal to $C[1] \cdot e^{-\theta \rho \omega_n}$, $\beta(\theta)$ equal to $C[2] \cdot e^{-\theta \rho \omega_n}$, and τ equal to $\sqrt{1-\rho^2}\,\omega_n$, which is the damped natural frequency of the absorber. Therefore, $a(\theta)$ in equation 3.1 is

equal to $\sqrt{\left(C[2] \cdot e^{-\theta \rho \omega_n}\right)^2 + \left(C[1] \cdot e^{-\theta \rho \omega_n}\right)^2}$, ϕ_1 is $ArcTan\left[\dfrac{C[2]}{C[1]}\right]$, and ω_1 is equal to

$\sqrt{1-\rho^2}\,\omega_n$. For the steady-state portion, set α equal to

$$\dfrac{\Gamma\left(\omega^2 - \omega_n^2\right)}{\omega^4 + 2\left(2\rho^2 - 1\right)\omega^2\omega_n^2 + \omega_n^4}, \quad \beta \text{ equal to } \dfrac{2\Gamma\rho\omega\omega_n}{\omega^4 + 2\left(2\rho^2 - 1\right)\omega^2\omega_n^2 + \omega_n^4}, \text{ and } \tau$$

equal to ω. Therefore, b in equation 3.1 is equal to

$$\sqrt{\left(\frac{2\Gamma\rho\omega\omega_n}{\omega^4 + 2\left(2\rho^2 - 1\right)\omega^2\omega_n^2 + \omega_n^4}\right)^2 + \left(\frac{\Gamma\left(\omega^2 - \omega_n^2\right)}{\omega^4 + 2\left(2\rho^2 - 1\right)\omega^2\omega_n^2 + \omega_n^4}\right)^2} \ , \ \phi_2 \ \text{is}$$

$ArcTan\left[\dfrac{2\rho\omega\omega_n}{\left(\omega^2 - \omega_n^2\right)}\right]$, and ω_2 is equal to ω.

    This resulting envelope amplitude, when plotted against θ, appears as an exponentially decaying, oscillation, which connects the local peak values of the absorber response. When the solution reaches steady state the envelope amplitude becomes constant, as one would expect. Figure 3-1 is an example of a plot of the analytical solution and the envelope equation with the parameter values set to be those listed in table 2-1.
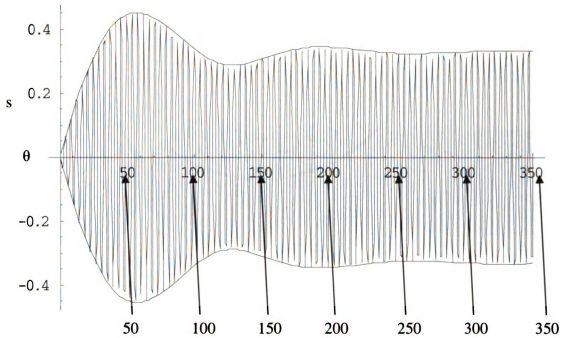

Figure 3-1: Plot of the envelope for the absorber, along with the absorber response, calculated from the linearized model.

This envelope equation is a useful design tool because it allows for easy identification of the maximum value of the transient oscillations and the maximum steady state value. The values are calculated by taking the derivative with respect to θ of the envelope equation, setting that derivative equal to zero, solving for θ, and plugging this value back into the envelope equation.

The same process can also be utilized on equation 2.17 to find the envelope for the linearized rotor velocity. This allows for identification of any problematic transient issues that could arise in the rotor as a result of the counter-torque being supplied by the absorber during transient operation. Figure 3-2 is a plot that shows the linearized rotor velocity encased by its envelope amplitude.
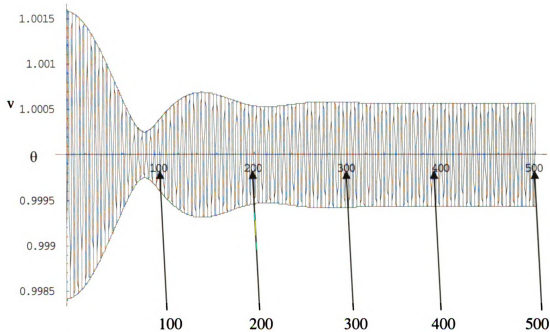

Figure 3-2 Plot of the envelope for the rotor velocity, along with the rotor velocity, calculated using the linearized model.

3.2 Decay Functions

A set of functions that conveniently describes the decay of the transients can be derived directly from the envelope equations. These functions $(a(\theta)+b)$ and $(b-a(\theta))$, where the values of $a(\theta)$ and b are the same as given in equation (3.1) of the preceding section [7]. These functions are described as decay functions because they both are purely decaying exponentials, that is, they have no oscillating components. The function $(a(\theta)+b)$ only contacts the amplitude function when it is at a maximum and $(b-a(\theta))$ only contacts the amplitude function when it is at a minimum. Figure 3-3 shows an example of how the decay functions appear relative to the envelope and the full absorber response, p. These decay functions lead to the insight that the decay rate of the envelope equation and the analytical solution for p is $e^{-\rho\omega_n\theta}$. Thus, the envelope has a time constant of $\dfrac{1}{\rho\omega_n}$. Of course, these results are also valid for the decay of the rotor transient.
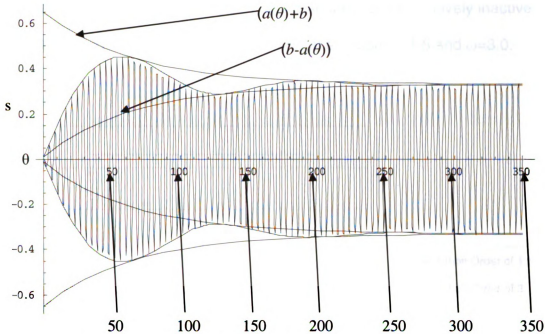
Figure 3-3: Plot of the decay functions, the absorber envelope, and the absorber response. all calculated using the linearized model.

3.3 Influence of Parameter Values

The peak value of the envelope equation can be used to determine trends that arise when properties such as the damping, the inertia ratio, and the order of the path are varied. This allows for more effective design practices and saves time and money that otherwise would be wasted on building and testing prototypes, or running detailed simulations.

In general, the worst case scenario for transients is to start the system with zero initial conditions for the absorbers. In this section we consider two such cases, motivated by MDS engine applications. The first case is when the excitation order is close to that of the absorber, that is, the absorber sees the excitation for which it is tuned. The other case is when the excitation order is

about twice that of the absorbers, that is, the absorbers are relatively inactive. In the present study these excitation orders are taken to be $\omega=1.5$ and $\omega=3.0$.

Figure 3-4: The effect of the absorber damping on the maximum transient absorber amplitude, calculated using the maximum value of the absorber envelope from the linear model.

Γ	0.04
ñ	1.51
ε	0.075
P_0	0
V_0	0

Table 3-1: List of system parameter values for figure 3-4

Figure 3-4 is based on using the values of table 3-1 in the envelope equation and varying the non-dimensional damping value of the absorber, μ_a. It

is seen that for ω=3.0 the absorber amplitude is very small and therefore the damping has little affect on the peak transient. However, when the excitation is ω=1.5, the transient absorber response is large and there is a sizable decrease in maximum transient absorber amplitude as the damping of the absorber increases.
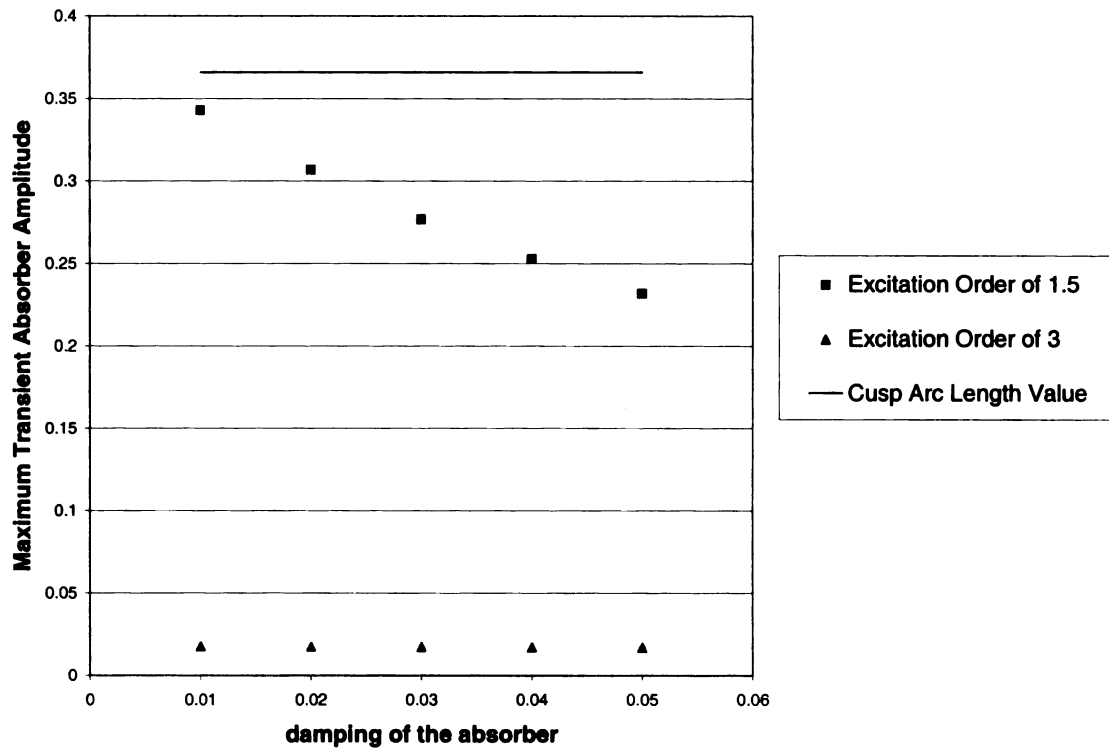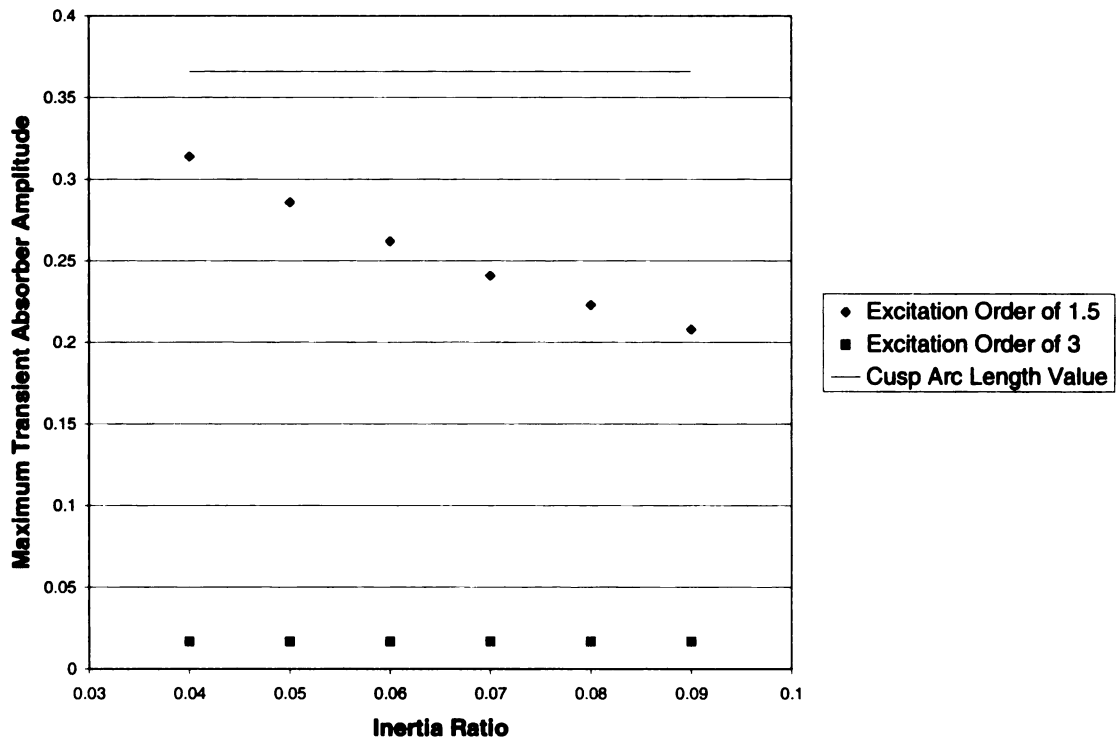

Figure 3-5: The effect of the inertia ratio on the maximum transient absorber amplitude, calculated using the maximum value of the absorber envelope from the linear model.

μ_a	0.05
$\bar{n}$	1.51
Γ	0.04
P_0	0
V_0	0

Table 3-2: List of system parameter values for figure 3-5

28

Figure 3-5 is a plot showing the dependence of the peak absorber transient amplitude and on the ratio of the absorber inertia to the rotor inertia using the values of table 3-2 for the other parameters. Figure 3-5 shows a similar decrease to that of figure 3-4 in maximum transient absorber value for the $\omega=1.5$ case, and very little effect for the $\omega=3.0$ case.
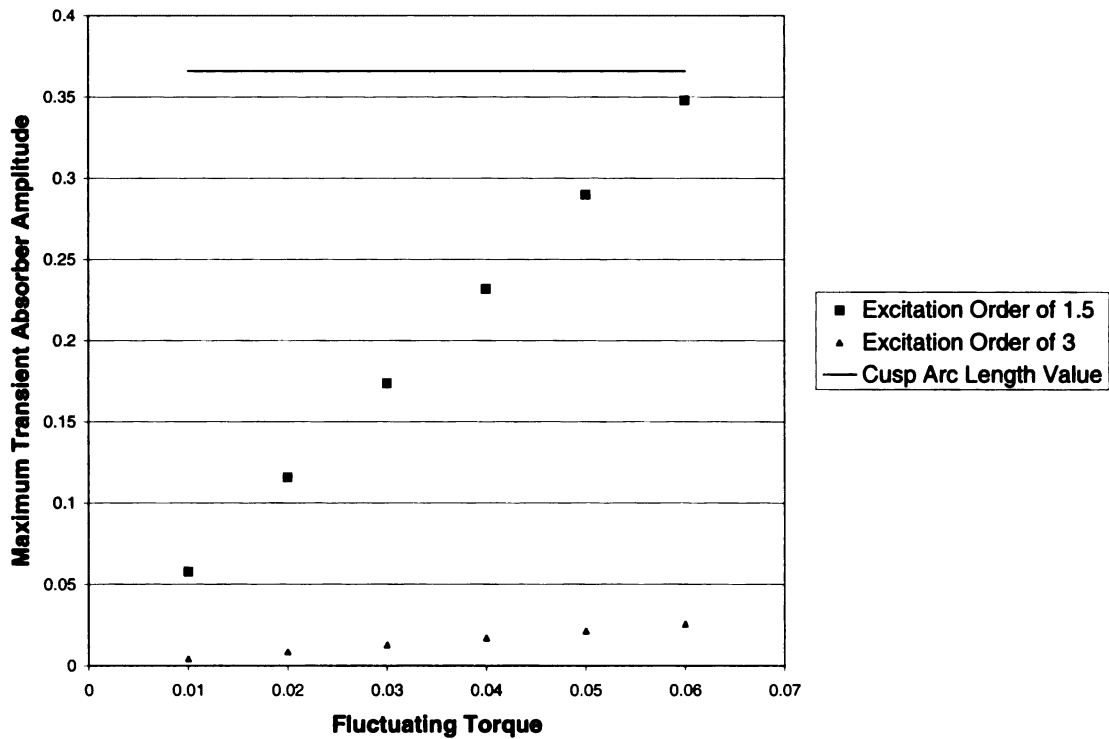

Figure 3-6: The effect of the fluctuating torque amplitude on the maximum transient absorber amplitude, calculated using the maximum value of the absorber envelope from the linear model.

μ_a	0.05
$\bar{n}$	1.51
ε	0.075
P_0	0
V_0	0

Table 3-3: List of system parameter values for figure 3-6

Figure 3-6 shows the effect of the fluctuating torque on the peak transient absorber amplitude. Since the system is linear, these results are linear, but it is seen that the ω=1.5 case is much more sensitive than the ω=3.0 case, as expected. Parameters for this plot are listed in Table 3-3.
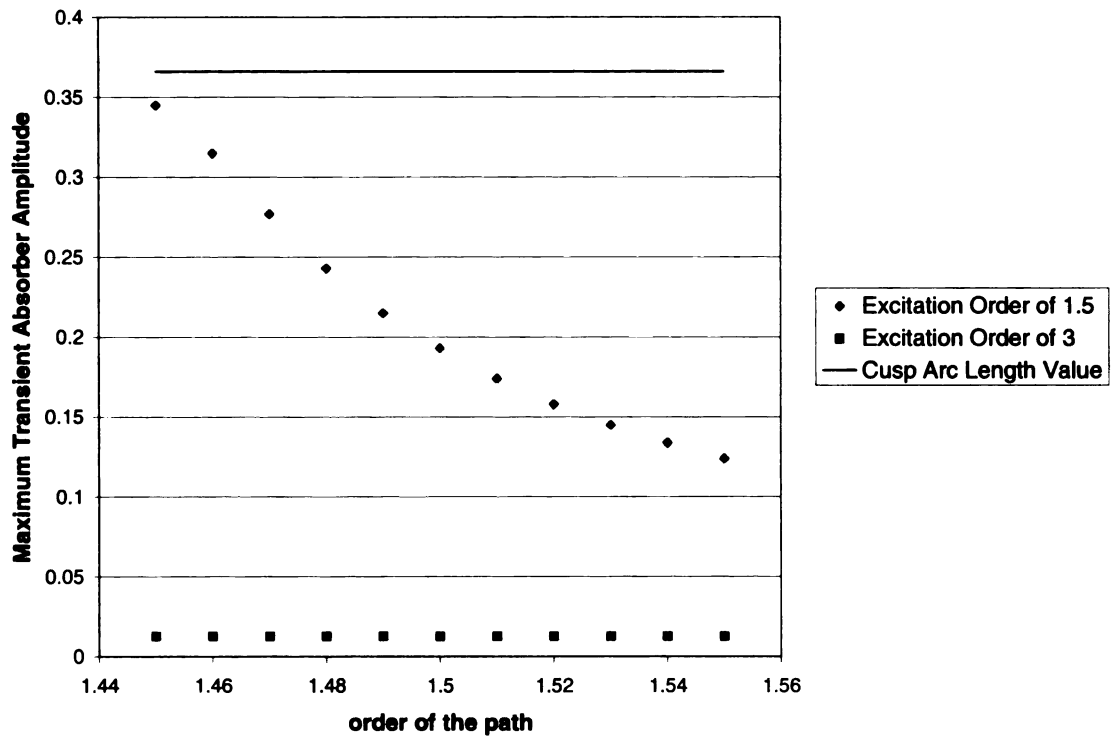

Figure 3-7: The effect of the absorber linear tuning on the maximum transient absorber amplitude, calculated using the maximum value of the absorber envelope from the linear model.

μ_a	0.05
Γ	0.03
ϵ	0.075
P_0	0
V_0	0

Table 3-4: List of system parameter values for figure 3-7

Figure 3-7 shows the influence of the absorber tuning order on the peak transient absorber amplitude. Again, for ω=3.0 the effect is negligible. For ω=1.5, note that large transients are observed if the system is undertuned, but that increasing the level of overtuning reduces the transient peak amplitude. This is not surprising, but the result gives a quantitative measure to the expected trend. This curve may be particularly helpful in selecting the absorber tuning order. Figure 3-7 was developed by using the values given in Table 3-4.

3.4 Changing the Excitation

Here we consider the case of interest for activation and deactivation of cylinders in an MDS engine. Recall that the excitation order is equal to one-half the number active cylinders, and this switches back and forth between $\dfrac{NC}{2}$ (k=2)

and $\dfrac{NC}{4}$ (k=1) for a four stroke engine, where NC is the number of engine cylinders. The absorber response appears as depicted in figure 3-8 when k switches from a value of 1 to 2.

31

Figure 3-8: Simulation of the absorber response when the excitation is switched away from resonance, calculated using the original nonlinear model.

Γ	0.04
$\bar{n}$	1.51
ε	0.05
μ_0	0.05
P_0	0
V_0	0

Table 3-5: List of system parameter values for figure 3-8.

Note that the case $k=1$ is close to the absorber resonant order, whereas $k=2$ is nearly twice the absorber resonant order. Figure 3-9 shows the case where k switches from a value of 2 to 1.
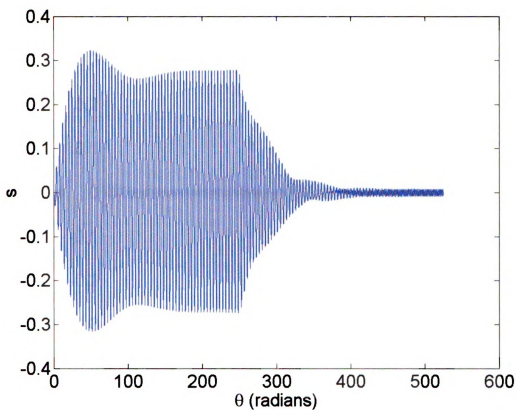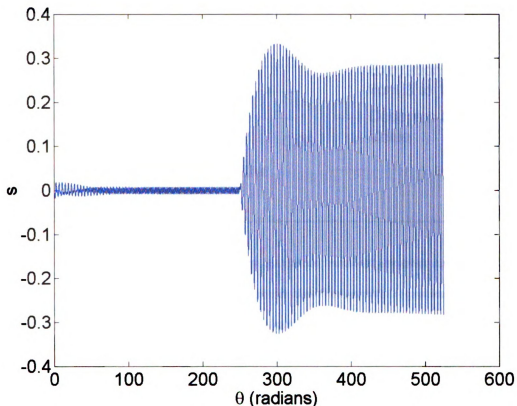
Figure 3-9: Simulation of the absorber response when the excitation is switched towards resonance, calculated using the original nonlinear model. The other system parameters are in table 3-5.

In figure 3-9, after the transition point, there is an over-shoot while the absorber moves to a new steady-state. This differs from the exponential decay seen after the transition point in figure 3-8.

Figure 3-10 shows a comparison of the effects of this changing excitation on the peak transient absorber amplitude, along with the steady state amplitudes, for different levels of absorber damping. For the k=2 to k=1 transition, several points are shown in the Figure, each of which represents a different starting phase from the k=2 response, that is, from different points on the ellipse shown in Figure 2-4.
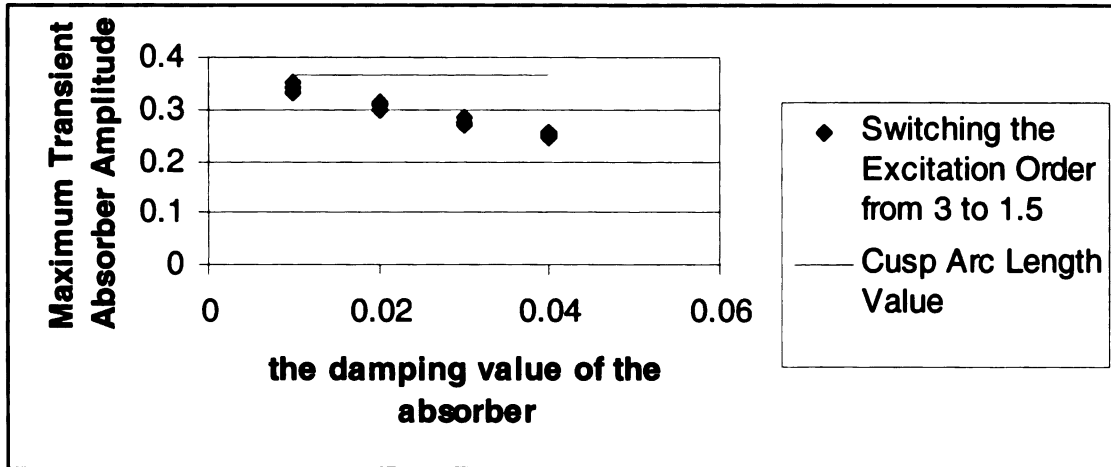
Figure 3-10: The influence of absorber damping on the maximum transient absorber amplitude when the excitation is switched toward resonance, from the absorber envelope equation, using different starting phases from the n=3 steady-state. Calculated using the values of table 3-1.

In figure 3-10, note that for the $k=2$ to $k=1$ transition, the maximum absorber transient value varies by some amount depending on the switching phase. This is represented by the scatter of maximum transient absorber amplitudes in this case. The largest of these values is the case of most importance, since it is the largest of the possible maximums. The details of this variability should be considered in the context of the actual application, which will dictate the switching phase.

Chapter 4

Averaging Analysis

Averaging is a method in which solutions of a certain class of nonlinear differential equations may be approximated. The method was developed initially by Krylov and Bogoliubov [8].

4.1 Averaged Equations

The method of averaging is applicable to systems in the following form [8],

$$\dot{x} = \varepsilon f(x,t,\varepsilon), \qquad x \in U \subseteq \mathfrak{R}^n, \ 0 \le \varepsilon \ll 1 \tag{4.1}$$

where f is T-periodic in t. The associated autonomous averaged system is as defined,

$$\dot{y} = \varepsilon \frac{1}{T} \int_0^T f(y,t,0) dt \overset{def}{=} \varepsilon \bar{f}(y) \tag{4.2}$$

Note that in the present application, the time variable is actually the rotor angle, θ. The equations are $\dfrac{2\pi}{n}$ periodic in θ, and the averaging will be carried out

35

accordingly. Before the non-dimensional equations of motion can be averaged, some scaling must be done to put these equations into the form of equation 4.1. First, the inertia ratio, ε, is considered to be small. This makes the coupling between the rotor and absorber relatively weak, and allows the uncoupling of the absorber equation from that of the rotor. Also new parameters are established in equation 4.3 [10], in order to reflect small damping and small excitation:

$$\mu_a = \varepsilon\tilde{\mu}_a, \qquad \mu_o = \varepsilon\tilde{\mu}_o, \qquad \Gamma_0 = \varepsilon\tilde{\Gamma}_0, \qquad l_k\Gamma_\theta = \varepsilon\tilde{\Gamma}_\theta \qquad (4.3)$$

The first order approximations of the absorber equations are [9],

$$s_i^{''} + \tilde{n}^2 s_i = \varepsilon f_i\left(s_1, ..., s_N, s_1', ..., s_N', \theta\right) + O\left(\varepsilon^2\right), \qquad 1 \le i \le N$$
where
$$f_i\left(s_1, ..., s_N, s_1', ..., s_N', \theta\right) = \qquad\qquad (4.4)$$
$$-\tilde{\mu}_a s_i' + [s_i' + \tilde{g}_i]\left[\frac{1}{N}\sum_{j=1}^{N}\left(-2\tilde{n}^2 s_j s_j' - \tilde{n}^2 \tilde{g}_i s_j + \frac{d\tilde{g}_j}{ds_j}s_j'^2\right) - \tilde{\Gamma}_\theta Sin[kn\theta]\right]$$

The forcing is considered to be near resonant. A detuning parameter is introduced to account for the differences between the excitation order and the linear tuning order of path of the absorber, which is defined as,

$$\Delta = \frac{\tilde{n}^2 - k^2 n^2}{\varepsilon} \qquad (4.5)$$

36

A transformation to slowly varying amplitude and phase variables is carried out as follows,

$$s = rCos[\varphi - kn\theta], \qquad s' = knrSin[\varphi - kn\theta] \tag{4.6}$$

Using this transformation in the equation of motion, in the standard approach [9], the resulting averaged equations for a single absorber are,

$$r' = \varepsilon \left(-\frac{1}{2}\tilde{\mu}_a r + \frac{\tilde{\Gamma}_\theta}{kn}Cos[\varphi]F_1(r) \right) + O(\varepsilon^2)$$

and

$$\varphi' = \frac{\varepsilon}{knr}\left(\begin{array}{c} -\tilde{\Gamma}_\theta Sin[\varphi]F_2(r) \\ +\frac{r\tilde{n}^2}{8}\left(r^2\left(3\tilde{n}^2\left(\tilde{n}^2+1\right)-k^2n^2\left(\tilde{n}^2+3\right)\right)-4\right)-\frac{r}{2}\Delta \end{array} \right) + O(\varepsilon^2) \tag{4.7}$$

where

$$F_1(r) = \frac{1}{2\pi}\int_0^{2\pi} Sin^2[x]\sqrt{1 - \left(\tilde{n}^2 + \tilde{n}^4\right)r^2Cos^2[x]}dx$$

$$F_2(r) = \frac{1}{2\pi}\int_0^{2\pi} Cos^2[x]\sqrt{1 - \left(\tilde{n}^2 + \tilde{n}^4\right)r^2Cos^2[x]}dx$$

In equation 4.7, the amplitude r describes the slowly varying envelope as described in Chapter 3, and it can therefore be used to find the maximum transient value of the absorber motion. The integrals in F_1 and F_2 are not

generally available in closed form; however, a Taylor expansion allows one to obtain series expansion solutions, as follows, out to fourth order in r,

$$F_1(r) = \frac{1}{128}\left(64 + \tilde{n}^2\left(1 + \tilde{n}^2\right)r^2\left(-8 - \tilde{n}^2\left(1 + \tilde{n}^2\right)r^2\right)\right) + O(r^6)$$

$$F_2(r) = \frac{1}{128}\left(64 + \tilde{n}^2\left(1 + \tilde{n}^2\right)r^2\left(-24 - 5\tilde{n}^2\left(1 + \tilde{n}^2\right)r^2\right)\right) + O(r^6)$$

(4.8)

Using equations 4.7 and 4.8, a numerical simulation can be created whose purpose is to numerically solve for r and φ and plot the slowly varying absorber amplitude r versus the angular orientation of the rotor. The numerical simulation was constructed in Matlab. Figure 4-1 shows a composite plot where the non-dimensional absorber arc length solved through a simulation of the full nonlinear equations is depicted in blue and the absorber amplitude envelope solved by a simulation of the averaged equations is depicted in green. This for a case when the excitation goes from resonant ($n=3$) to resonant ($n=1.5$).
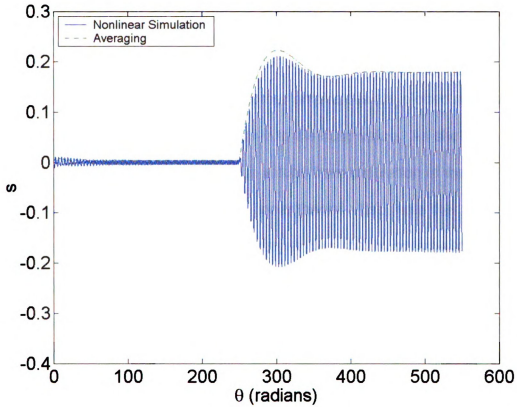
Figure 4-1: Simulation of the absorber response using the original nonlinear equations and an envelope calculated using averaging.

Γ	0.03
n̄	1.51
ε	0.05
μ₀	0.05
P₀	0
V₀	0

Table 4-1: List of system parameter values for figure 4-1

Using these results and those found in chapter 3, a comparison can be drawn as to the effectiveness of averaging and linear theory for approximating the solution of the largest transient absorber vibration amplitude. The test of the effectiveness of these methods is how close their results are to that of a

numerical simulation of full nonlinear equations of motion. The plot of this comparison is shown for different values of non-dimensional fluctuating torque in figure 4-2. Each value of fluctuating torque is used to solve for a different steady state solution. Maximum transient absorber amplitudes are plotted against the ratio of each steady state solution relative to the cusp value. As shown in the figure, averaging is slightly closer to the values from simulation of the full nonlinear equations than the results of linear theory. Also, note that the deviations occur only at relatively large amplitudes, that is, at large torque levels. Additionally, the results for large steady-state amplitudes, near the cusp value, from averaging and linear theory slightly exceed the cusp value. This is, of course, not possible, but the data provides a useful upper bound. The plot also shows that the two analytical methods can be considered conservative estimates, since each value over-estimates the actual value produced by the nonlinear simulation. The parameter values are set to those of table 4-2.
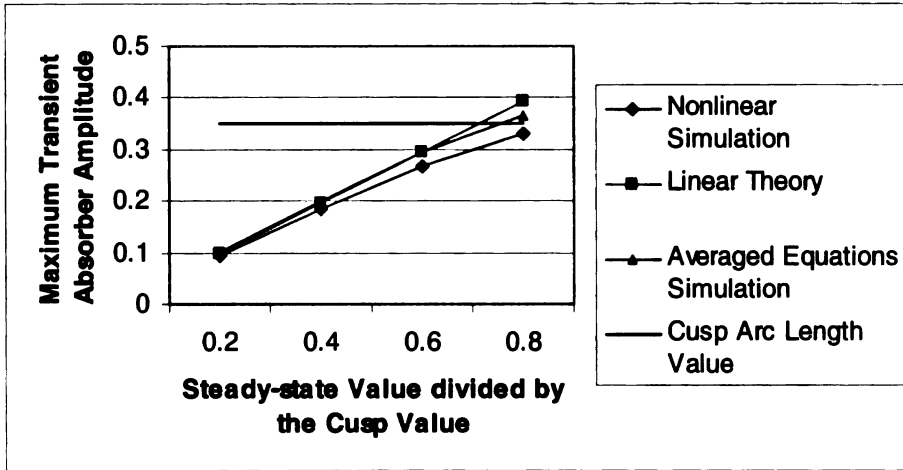
Figure 4-2: Comparison of the maximum transient absorber arc length found using simulations of the full nonlinear equations, linear theory, and averaging for different fluctuating torque values; with trend-lines added for clarity.

μ_a	0.05
ε	0.05
ω	3->1.5
$\bar{n}$	1.55

Table 4-2: List of system parameter values for figure 4-2

An alternative view of this comparison is in figure 4-3, which shows the non-dimensional absorber arc length solved through a simulation of the linearized equations, depicted in red, which is overlaid on top of the plot shown in figure 4-1.
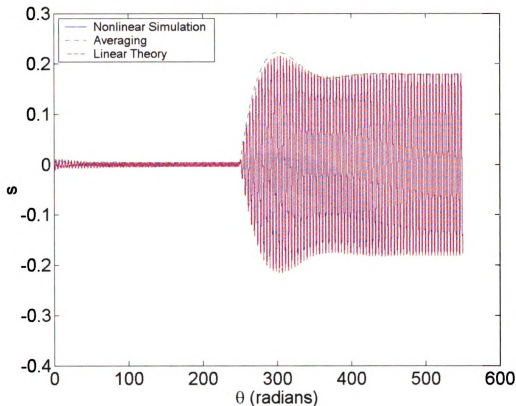
41

Figure 4-3: Comparison of the envelope from averaging, the absorber response calculated using the linearized model, and simulations of the full nonlinear equations; transition to resonance. Calculated using the values of table 4-1

The comparison can also be depicted in a third form in the phase plane as shown in figure 4-4. In the plot, the response based on linear theory is in red, based on averaging is in green, and based on the full nonlinear equations in blue. The averaging results were calculated using the transformation in equation 4.6. In the center of the phase plane plot, there is an area of tight swirling; this is when the absorber is settling down to a small amplitude steady-state, far from resonance. When the plot breaks out into a much larger swirling pattern, it is because the excitation has been changed and the absorber is being driven close

to resonance. Note that the response overshoots and the amplitude oscillates as it settles towards the new, large amplitude steady state.
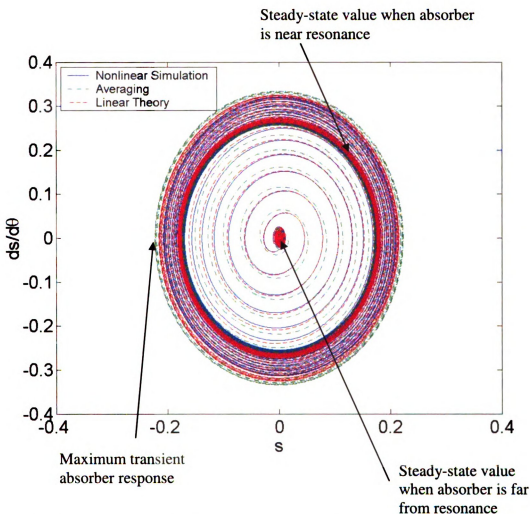

Figure 4-4: Transient responses in the phase plane of the absorber response, calculated by simulating the full nonlinear equations, the averaged equations, and from the linearized model. Calculated using the values of table 4-1

4.2 Influence of Parameters

Since it has been determined that the averaging approach is an accurate method, the effects of the damping, inertia, and order of the path of the absorber influence transient behavior from chapter 3 may now be revisited. Figures 4-5 a and b show that the trends that are seen using linear theory are also observed using averaging. These figures were created using the same parameter values as those used in chapter 3.
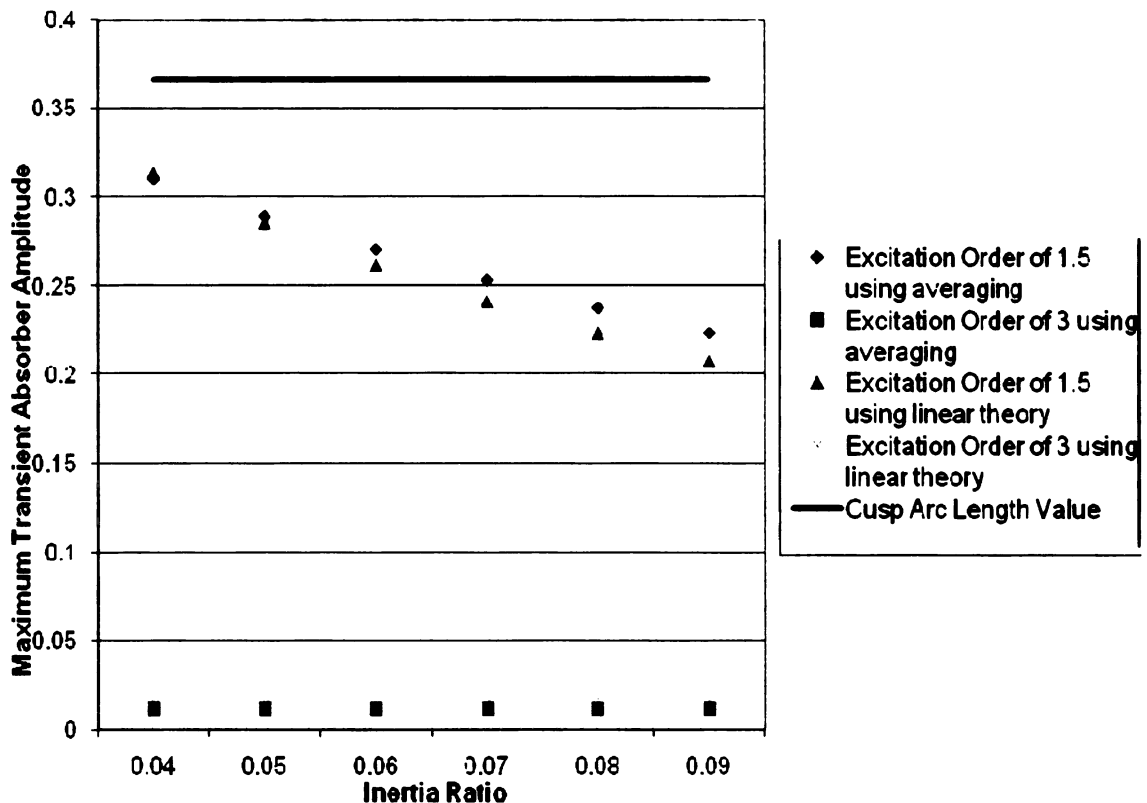

Figure 4-5 a: The effect of the inertia ratio on the maximum transient absorber arc length, calculated using the maximum value of the absorber envelope from linear theory and from averaging. Solved for using the values in table 3-2.
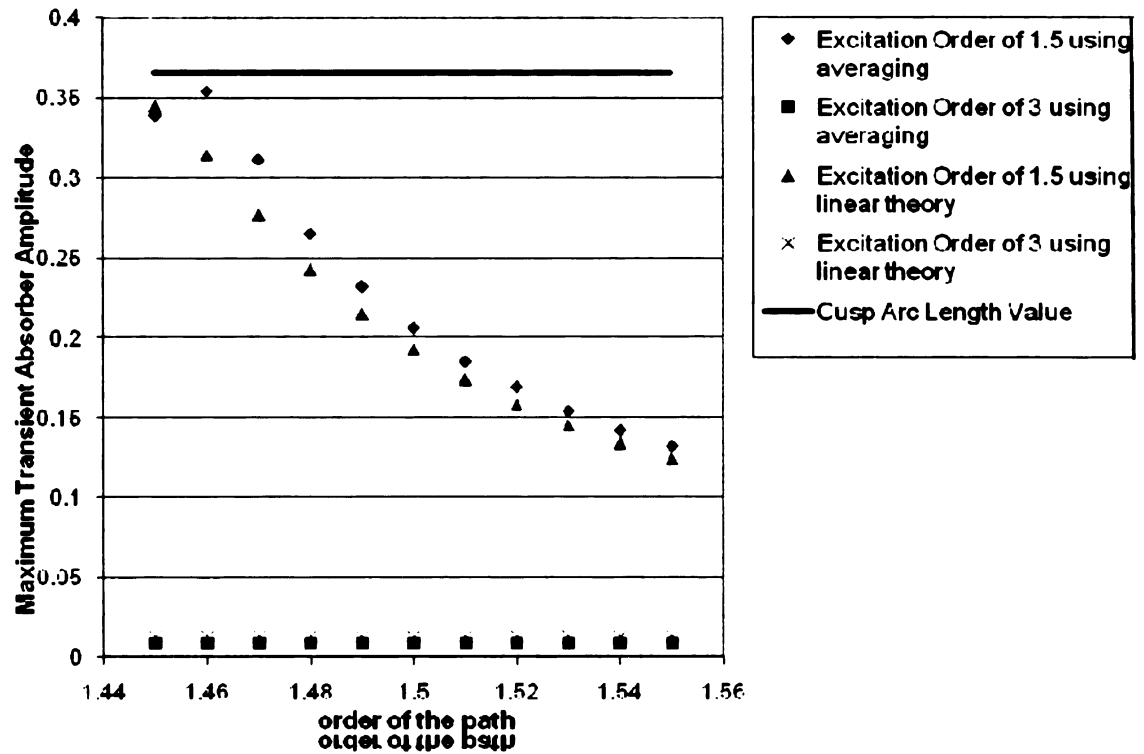
Figure 4-5 b: The effect of absorber linear tuning order on the maximum transient absorber response, calculated using the maximum value of the absorber envelope from linear theory and from averaging. Solved for using the values in table 3-4.

Chapter 5

Conclusions and Directions for

Future Work

The purpose of this study was to develop a better understanding of transient vibrations for centrifugal pendulum vibration absorbers with tautochronic epicycloidal paths, and to develop tools to predict the behavior of the absorber and rotor during transient response. Of particular interest are the peak amplitudes of the absorber motions and the rotor torsional vibrations, as these must be minimized in practice. Also, the study investigated the influence of certain parameters on these transient vibrations. This investigation was successful in accomplishing these goals, and it demonstrated that the simple linearized theory is quite good for predicting the transient vibrations of a CPVA for a wide range of operating conditions. This information sets the stage for further work on transient motions, including experimental work, more detailed simulations studies, and testing in automotive engines.

5.1 Summary of Results

The first methodology developed in this study for predicting the transient behavior of centrifugal pendulum vibration absorbers is to analyze the linearized

equations of motion for the system. Their solution yields expressions for the motion of the vibration absorber and the rotor velocity. The most important facets of the behavior, the maximum values of the absorber amplitude and rotor velocity, are found by utilizing trigonometric identities to develop equations that govern the slowly-varying amplitude envelope of these responses. Additionally, decay functions can also be derived from these results, which provide useful information about how the transient behavior decays.

The second methodology utilizes averaging. This involves a particular scaling of the system parameters and a transformation to absorber amplitude and phase coordinates, so that averaging can be applied. The resulting averaged equations, which also predict the slow-time envelope behavior, are studied via numerical simulations, from which one can determine the largest amplitude values.

A comparison of these two methodologies against simulations of the full equations of motion suggests that both are useful for approximating the solution of the nonlinear equations. In addition, the methods require much less computing power and time than simulating the full nonlinear equations outright. While averaging at times resulted in a better approximation to the actual solution, linear theory is simpler and nearly quite as accurate.

The study established the influences of the absorber damping, the absorber tuning, and the absorber inertia on the maximum transient amplitude of the absorber. As expected, it is seen that increasing the absorber damping, the absorber order (if overtuned), and the absorber inertia, all have the effect of

reducing the peak transient amplitude. The main advantage of this study is that the results allow one to quantify such effects. Also, these parameter relationships are not linear, and, therefore, as the parameter values get larger, a point of diminishing returns arises. In addition, higher damping lowers the effectiveness of the absorbers, since they eventually become just extra mass attached to the rotor, so a trade-off must be considered when influencing the damping. Similarly, as one overtunes the absorber, its effectiveness is diminished. Also, there is a limit to the amount of absorber mass one can use in a given application. So, tradeoffs must be made in the selection of these parameters when considering transient response. In addition, of course, one must keep in mind their effect on the steady-state performance of the absorbers.

5.2 Possible Areas of Future Study

The primary area for future study is generally in conducting experiments. Prototypes of these absorbers have already been manufactured by the DiamlerChrysler Corporation, one of which is depicted in figure 5-1. Figure 5-2 depicts the MSU testing setup with two of these prototypes attached to the rotor.
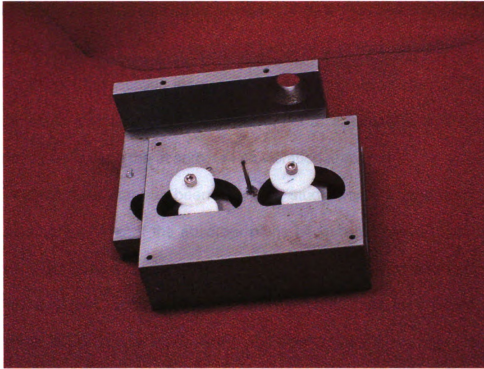
Figure 5-1: Photograph of a prototype bifilar CPVA.

The prototypes are called bifilar absorbers because they have two suspension points, via rollers that move along paths dictated by the shapes of holes machined in the surfaces of the absorber and the support flange fixed to the rotor. This absorber system, fitted on the MSU test rig, will be used in future studies of the transient response. The work described in this thesis provides the analytical background for these investigations.

The first test would be to run the rotor with an absorber attached and measure the largest transient amplitude value of the absorber. With these results a comparison may be made with the theoretical results produced in this study. The next test would be to implement multiple absorbers which are nearly identical. The reason to conduct such a test is to determine whether or not non-

synchronous transient responses can occur. It is known that non-synchronous steady-state responses can occur, as the result of dynamic instabilities [13], and that the effects of production inaccuracies exaggerate these effects [12]. Such behavior would diminish the effectiveness of the absorbers and, in a worst case scenario, can even turn the absorbers into vibration amplifiers.

Another area that has been yet to be studied is how long term use will affect these absorbers. If the absorber paths become worn over time, this can influence the parameter values, which will affect the transient and steady-state behavior, as shown in chapters 3 and 4. These absorbers have been used for many years in aerospace applications, where rotor speeds are nearly constant, and the issue of wear in the more transient automotive environment remains an outstanding question.
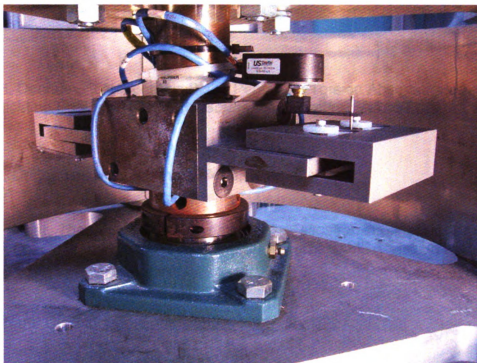
Figure 5-2: Photograph of the prototype testing setup.

References

[1] H. H. Denman, "Tautochronic Bifilar Pendulum Torsion Absorbers for Reciprocating Engines," *Journal of Sound and Vibration*, Vol 159 (2), p. 251-277, 1992.

[2] B.C. Carter. British patent no.337446, 1929.

[3] D. Palmer, *Theoretical and Experimental Investigation into the Transient Behavior of Centrifugal Pendulum Vibration Absorbers*. MS Thesis, Michigan State University, 2005.

[4] Wolfram. Cycloid. http://mathworld.wolfram.com/Cycloid.html.

[5] Wolfram. Epicycloid. http://mathworld.wolfram.com/Epicycloid.html.

[6] A. S. Alsuwaiyan and S. Shaw, "Performance and Dynamic Stability of General Path Centrifugal Pendulum Vibration Absorbers," *Journal of Sound and Vibration*, Vol 252 (5), p. 791-815, 2002.

[7] J. P. Den Hartog, *Mechanical Vibrations*. Dover Publications, 4th edition, 1984.

[8] J. Guckenheimer and P. Holmes, *Nonlinear Oscillations, Dynamical Systems, and Bifurcations of Vector Fields*. Springer-Verlag, 1983.

[9] P. M. Schmitz, *Experimental Investigation into Epicycloidal Centrifugal Pendulum Vibration Absorbers*. Master's thesis, Michigan State University, 2003.

[10] C. P. Chao and S.W. Shaw, "The Dynamic Response of Multiple Pairs of Subharmonic Pendulum Vibration Absorbers," *Journal of Sound and Vibration*, Vol 231 (2), pp. 411-431, 2000.

[11] S. Shaw and C. Pierre, "The Dynamic Response of Tuned Impact Absorbers for Rotating Flexible Structures," Journal of Computational and Nonlinear Dynamics, Vol 1 (1), p.13-24, 2006.

[12] A.S. Alsuwaiyan and S.W. Shaw, "Steady-State Response of Systems of Nearly-Identical Torsional Vibration Absorbers," *Journal of Vibration and Acoustics*, Vol 125, pp. 80-87, 2003.

[13] C.-P. Chao, C.-T. Lee, and S.W. Shaw, "Non-Unison Dynamics of Multiple Centrifugal Pendulum Vibration Absorbers," *Journal of Sound and Vibration*, Vol 204 (5), pp. 769-794, 1997.

[14] C.-P. Chao, C.-T. Lee, and S.W. Shaw, "Stability of the Unison Response for a Rotating System with Multiple Centrifugal Pendulum Vibration Absorbers," *Journal of Applied Mechanics*, Vol 64, pp. 149-156, 1997.